16TH EUROPEAN CONFERENCE ON EARTHQUAKE ENGINEERING THESSALONIKI 18 - 21 JUNE 2018

EXPLAINING THE ANOMALOUS DAMAGE PATTERN OF LARGE (M7+) INTERMEDIATE-DEPTH EARTHQUAKES IN THE SOUTHERN AEGEAN SEA

Charalampos KKALLAS[1], Constantinos PAPAZACHOS[2], Andreas SKARLATOUDIS[3], Chrysanthi VENTOUZI[4], David BOORE[5], Basil MARGARIS[6]

ABSTRACT

During the 19th and early 20th century four large (**M**7+) events occurred in the eastern Cretan basin area (southern Aegean Sea). These events (1810 **M**~7.5, 1856 **M**~7.7, 1887 **M**~7.2, and 1935 **M**~7.0) had a very characteristic, anomalous damage patterns, as they were moderately felt in their epicentral region (virtually unfelt in the broader back-arc Aegean Sea area), while they were strongly experienced throughout the whole eastern and central Mediterranean (Cyprus, Egypt, Italy, Malta). Their most significant impact was systematically observed at relatively large epicentral distances (>100-120 km) along the southern and eastern Hellenic arc, with heavy damage in the islands of Crete and Rhodes. For example the 1856 (**M**~7.7) earthquake had a 500+ death toll, destroying or damaging more than 20,000 houses in central Crete (e.g. Papazachos and Papazachou, 2003).
The previously described macroseismic field strongly suggests that all these four events were intermediate-depth earthquakes: The anomalous damage pattern is mainly due to strong attenuation along the volcanic-arc (back-arc) area and the selective seismic energy propagation through the low-attenuation eastern Mediterranean subduction beneath the Aegean Sea. To confirm this, we examine the damage pattern of the largest, 1856 (**M**~7.7) earthquake, using a combination of Ground-Motion Prediction Equations (GMPE) and stochastic simulations, appropriately adapted for these events. The results obtained are in good agreement with the observed macroseismic data, confirming the enhanced impact of such events in the fore-arc islands of the entire central and eastern Hellenic arc.

Keywords: Historical earthquakes; Stochastic simulation; GMPE; Intermediate-depth earthquakes; Southern Aegean; Hellenic subduction.

1. INTRODUCTION

Obtaining reliable epicenter information for historical intermediate-depth earthquakes in the Aegean

[1] M.Sc. Seismologist, Aristotle University of Thessaloniki, Thessaloniki, Greece, chkkalla@geo.auth.gr
[2] Professor, Aristotle University of Thessaloniki, Thessaloniki, Greece, kpapaza@geo.auth.gr
[3] Ph.D. Seismologist, Aristotle University of Thessaloniki,Thessaloniki, Greece, askarlat@auth.gr
[4] Ph.D. Seismologist, Aristotle University of Thessaloniki, Thessaloniki, Greece, xrusven@geo.auth.gr
[5] Ph.D. Seismologist, U.S. Geological Survey, California, U.S, dboore@yahoo.com
[6] Research Director, Institute of Engineering Seismology & Earthquake Engineering (EPPO-ITSAK), Thessaloniki, Greece, margaris@itsak.gr

Sea area is a difficult task, mainly due to the spatially anomalous distribution of their macroseismic intensities, as well as the absence of instrumental data. This anomalous damage pattern is mainly the result of the low velocity-high attenuation layer beneath the volcanic arc at the depth range of 60-90 km (e.g. Ventouzi et al., 2015). However, the combination of historical data (e.g. macroseismic intensities) with results obtained from GMPEs and stochastic simulations can contribute to a better understanding and assessment of historical intermediate-depth earthquake information (e.g. Skarlatoudis et al., 2013; Kkallas et al., 2018a,b).

The previously described high attenuation area is typically attributed to the presence of melt and/or significant volatile content at the depth of 60-90 km, due to the subduction of the Mediterranean lithospheric plate under the Aegean microplate, leading to the strong attenuation of S (but also P) waves along the South Aegean Sea volcanic-arc (e.g. Papazachos et al., 2005). More specifically, the Aegean microplate is moving towards the southwest with an average velocity of ~35 mm/yr with respect to stable Europe, while the Mediterranean plate moves towards Europe at a rate ~5-10 mm/yr, subducting under the Aegean (Fig.1). As a result, intermediate-depth earthquakes occur along a well-defined Benioff zone in the South Aegean Sea (see isodepth lines in Figure 1), occasionally with large magnitudes. A typical example is the historical earthquake of 1856 (**M**~7.7), for which significant damage was observed mainly in Crete, while in the back-arc area (e.g. islands of Santorini and Amorgos), limited damage was reported. This damage pattern is due to the specific mantle wedge attenuation pattern, which causes large differences between fore-arc and back-arc sites. Figure 1 presents two possible epicenters for the 1856 historical intermediate-depth event (from Papazachos, 1996 and Papadopoulos et al., 2011). As various epicenters and magnitudes have been assigned to this event by different authors, we determine a reliable hypocenter and magnitude by reevaluating the available information, in order to better model the damage pattern of this important event.

The selected event is one of the most destructive earthquakes which ever occurred in the southern Aegean Sea, as ~600 people died, and many others were injured. In Crete, 538 people died and 638 were injured, while in the islands of Rhodes and Karpathos 60 and 20 people died, respectively. Overall, in Crete 11317 houses suffered damage and 6512 collapsed. The largest macroseismic intensities were recorded in the Heraklion city, since only 18 from the 3620 city houses remained habitable. In the city of Chania, several people died or were injured, while in Rethymno all houses suffered moderate to significant damage. In Sitia, Ierapetra and Myrampelou many houses collapsed. Neighboring islands were significantly affected, with 2000 and 8000 houses collapsing in the islands of Rhodes and Karpathos, respectively. In the island of Kasos three villages suffered serious damage, extensive damage was recorded in Simi, Kastelorizo, Amorgo and Cyprus, while in Santorini, some churches also collapsed (see Papazachos and Papazachou, 2003 for detailed descriptions).

The damage description of the 1856 event suggests that such events constitute a major source of seismic hazard for southern Aegean urban areas (Heraklion, Rhodes city, etc.), where building practices have resulted in a large number of multi-story constructions. Since this infrastructure has not experienced such events, due to the lack of M7+ intermediate-depth earthquakes in the study area for the last ~100 years, it is clear that additional focused studies are necessary to better assess the spatial variability of the seismic motion, highlighting areas that will be affected by future M7+ intermediate-depth events.

In this work, we use local or locally adapted (Skarlatoudis et al., 2013, Skarlatoudis, 2017) and global (e.g. Abrahamson et al., 2015) GMPEs, that can account for back-arc/fore-arc variations for intermediate-depth events. We also employ stochastic simulations using the finite-fault stochastic method, as modified by Boore (2009). The strong ground-motion attenuation model and source properties for these simulations are based on recent results (Kkallas et al., 2018a) from the analysis of intermediate-depth strong-motion data for the study area. Furthermore, we examined the applicability of a recently proposed 3D tomographic attenuation (Q_S) model for the area, to better constrain the high-frequency spectral decay for the performed simulations. Predicted ground motions (e.g. PGA and PGV) are calibrated with historical information in terms of macroseismic intensities, available from the observed damage distributions. While some source parameters (magnitude, fault geometry, stress parameter) are based on previous work conducted for the south Aegean Sea subduction area, we perform a hypocenter parametric investigation. Site effects are taken into account through a generic site amplification approach, using V_{S30} from topographic slope proxies, as adapted by Stewart et al. (2014) for the area of Greece.

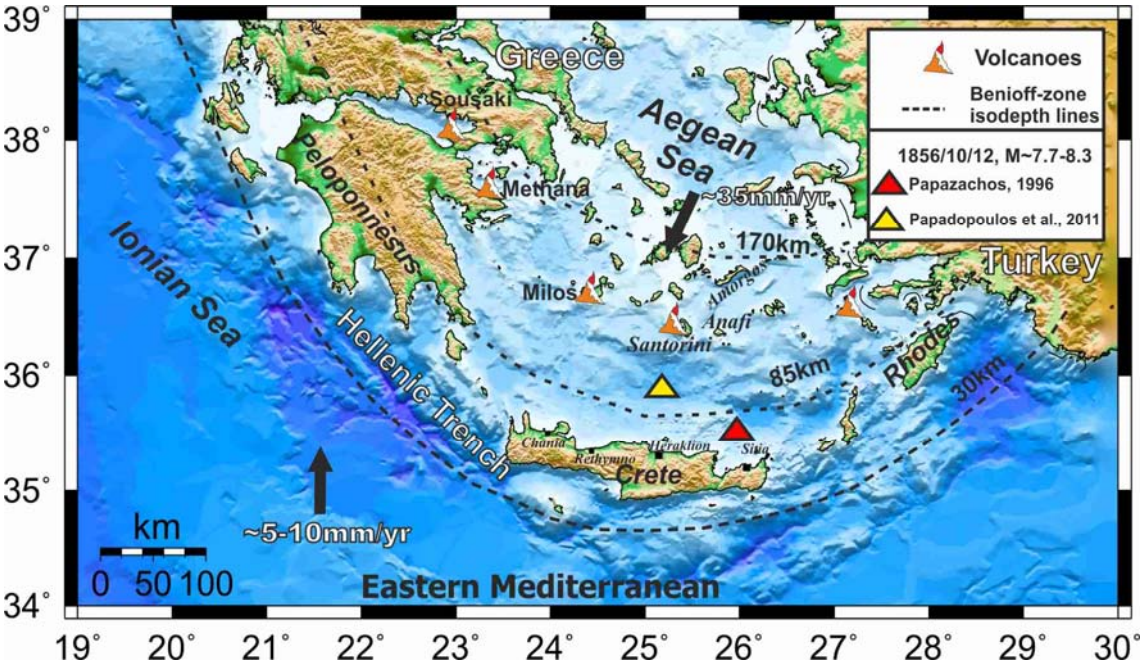

Figure 1. Geotectonic map of the southern Aegean Sea subduction. The main volcanic centers of the southern Aegean Sea volcanic arc, as well as two previously proposed epicenters for the 1856 intermediate-depth event are also presented.

2. STUDY REGION AND DATA PROCESSING

On October 12, 1856, an **M**~7.7-8.3 intermediate depth earthquake occurred north of Crete causing damage far away from its proposed epicenter. Maximum reported macroseismic intensities for this earthquake vary between 8 to 11, according to Sieberg (1932). As the original Intensity Data Points (IDP) are not available, we used information only from the reported isoseismal lines. For this reason, we digitized the isoseismal lines of the 1856 earthquake reported by Sieberg (1932) and generated a 2D regular macroseismic intensity grid. We then selected ~150 randomly distributed sites in the Southern Aegean Sea area, which simulate the possible IDP distribution. Figure 2a shows the isoseismal map of Sieberg (1932) (as redrawn by Jusseret et al., 2013), while Figure 2b shows the reconstructed map from the digitized isoseismal lines of Figure 2a. The randomly selected IDP locations are depicted with circles. It should be noted that denser IDP locations were selected in vicinity of areas exhibiting higher damage levels (e.g. the city of Heraklion). In general, the reconstructed macroseismic intensities (and the original isoseismals) are in excellent agreement with the expected damage pattern of intermediate-depth earthquake of the Southern Aegean subduction zone, since the largest macroseismic intensities are observed in the fore-arc area (north and east coasts of Crete, Karpathos, Rhodes), at a significant distance from the epicenter (e.g. >80 km), while at similar distances in the back-arc area seismic energy is strongly attenuated.

3. ASSESSMENT OF THE POSSIBLE 1856 EARTHQUAKE EPICENTER

Considering the low accuracy of historical seismicity locations and magnitude assessments, which is even poorer for intermediate-depth earthquakes for which maximum damage is not observed in the epicentral area, we initially attempted to constrain the earthquake location using available GMPEs for the intermediate-depth earthquakes of the study area. For this investigation, we employed a dense grid of possible hypocenters (spacing ~10 km for latitude-longitude and ~5 km for depth) covering the

study area (Figure 1), with a moment-magnitude range between 7.6 and 8.3. For the hypocentral depth, we adopted the theoretical Benioff zone geometry proposed by Vamvakaris et al (2016), allowing for a ±10 km maximum depth deviation from the proposed geometry.

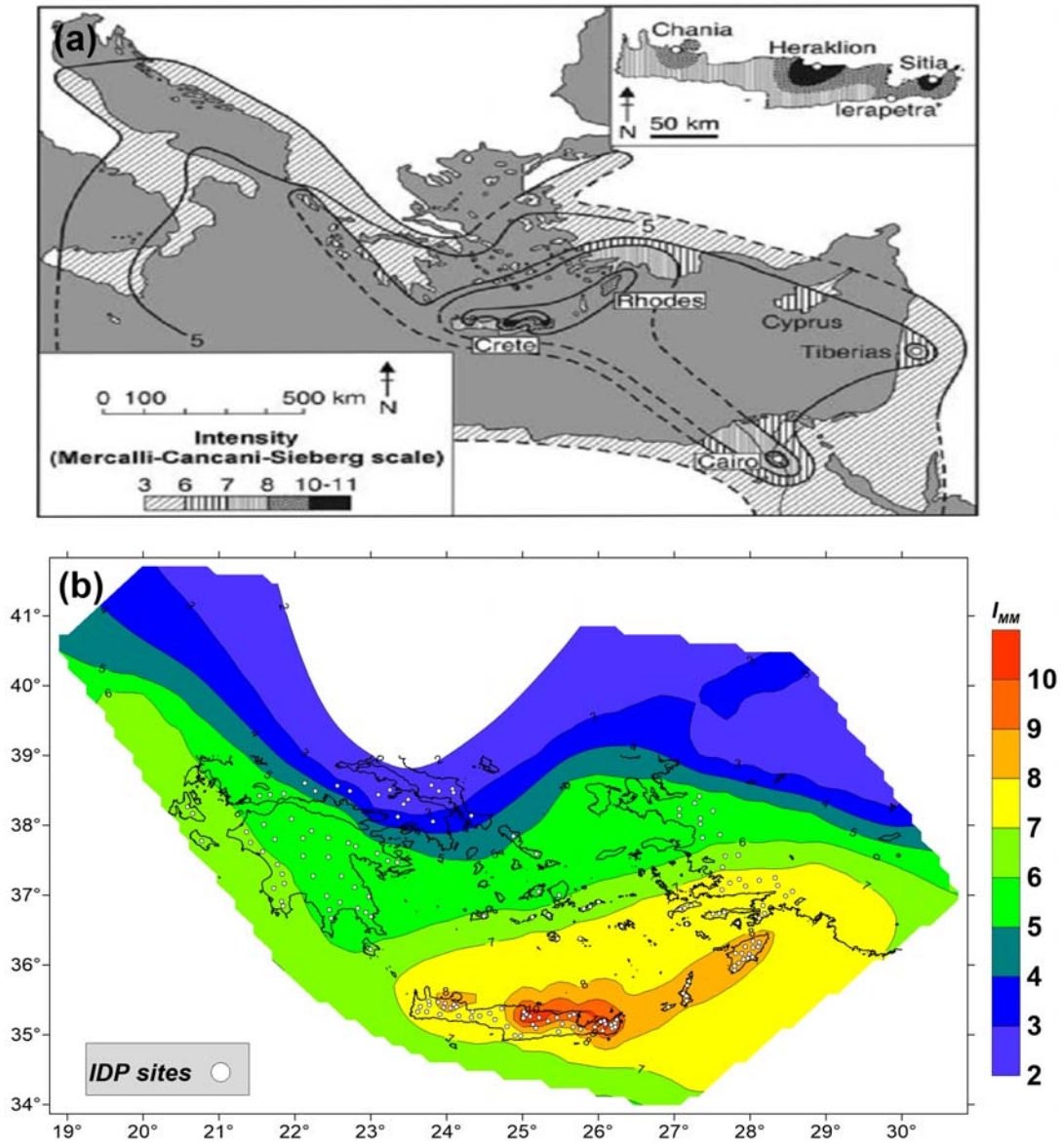

Figure 2. (a) Isoseismal map of the 12 October 1856 earthquake, redrawn after Sieberg (1932) from Jusseret et al. (2013). b) Reconstructed isoseismal map based on Figure 2a, used in the present work. The 150 randomly sampled virtual IDP are depicted with open circles.

For each possible hypocenter location, we have estimated the peak ground acceleration (PGA) for each digitized IDP, using three GMPEs for intermediate-depth earthquakes proposed for the study area from Skarlatoudis et al. (2013) and Skarlatoudis (2017). To convert synthetic PGA values to macroseismic intensities used equation (1), proposed for intermediate-depth earthquakes in the southern Aegean Sea region (Kkallas et al., 2018b).

$$\boldsymbol{I} = \begin{cases} 2.20 * log_{10}(PGA) + 1.5, \ if \ 4.8 \leq PGA(cm/s^2) < 66 \\ \\ 3.66 * log_{10}(PGA) - 1.16, \ if \ PGA(cm/s^2) \geq 66 \end{cases} \quad (1)$$

Figure 3 presents the spatial distribution of the 100 best epicenters from ~14000 initially generated hypocenter candidates, showing the smallest RMS and bias values. The smaller RMS misfit and bias is observed in Figure 3a, which is based on the model of Skarlatoudis et al. (2013) that was originally proposed for intermediate-depth earthquake modelling for the southern Aegean Sea region. This GMPE accounts for different fore-arc and back-arc attenuation patterns, nicely capturing the main features of the damage distribution in the area. The modified equations of Zhao et al. (2006) and Abrahamson et al. (2015) models, as adapted for the southern Aegean by Skarlatoudis et al. (2017), show larger values of RMS and bias than the Skarlatoudis et al. (2013) model, with the Abrahamson et al. (2015) BCHydro model showing a better performance. On the other hand, both these models suggest a smaller magnitude (**M**=7.7) compared to the **M**=8.3 proposed in Figure 3a.

Significant differences are also observed when considering the proposed earthquake location. The regional Skarlatoudis et al. (2013) GMPE proposes a hypocenter in the broader Santorini-Anafi area, while the adapted Zhao et al. (2006) GMPE proposes a hypocenter closer to eastern Crete, with shallower depth. Finally, the adapted BCHydro GMPE of Abrahamnson et al. (2015) has two local minima, at both previously proposed locations.

In Figure 3d we present the best (smallest RMS) epicenter from each of the two clusters (with red triangles), as well as typical fault plane solutions for each hypocenter from the work of Kkallas et al. (2013). In the same plot, we also present the epicenters for the 1856 earthquake previously proposed by other researchers, as well as the epicenters for the intermediate-depth induced aftershock (**M**~6.9) of the 1956 Amorgos (**M**=7.5) event (the latter being a normal shallow earthquake). It is clear that the first candidate epicenter is located close to 1956 aftershock area, which was an induced event on the Benioff zone by its normal (shallow) tectonic mainshock.

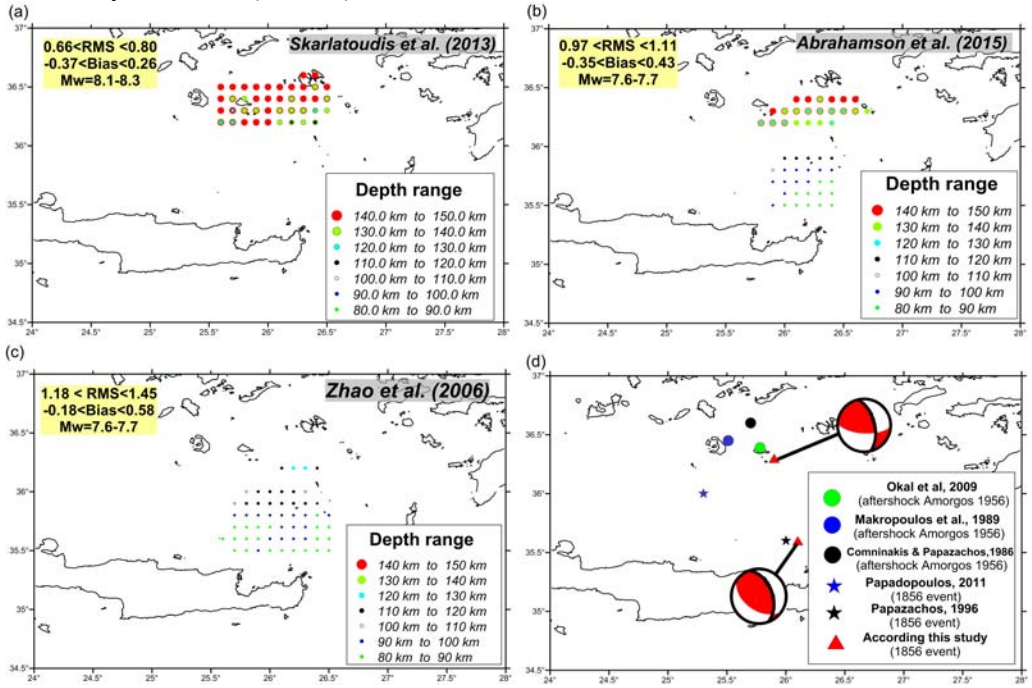

Figure 3. Possible hypocenters of the 1856 event as estimated by macroseismic data fit using (a) the regional GMPE of Skarlatoudis et al. (2013) and, the global relations of (b) Abrahamson et al. (2015) and (c) Zhao et al. (2006), as adapted for the Aegean Sea by Skarlatoudis (2017). For each family of solutions, the range of macroseismic intensity RMS and bias (between observed and modeled intensity values) is also reported for comparison. d) Best-fit locations of the 1856 event (red triangles) from previous plots, together with the corresponding typical intermediate-depth Fault Plane Solutions for the two areas. Locations for the same earthquake by other researchers, as well as the 1956 induced intermediate-depth aftershock of the large Amorgos 1956 (**M**~7.5) tectonic event are also shown, for comparison. Thick black lines on the focal mechanisms depicts the fault plane adopted for stochastic simulations, as presented later.

Figures 4 and 5 present the distribution of RMS and bias values for the two best-fit locations depicted in Figure 3d (h=90 km, **M**=7.7 and h=130 km, **M**=8.3) for the regional GMPE of Skarlatoudis et al

(2013) and the adapted for the Aegean BCHydro GMPE. We have excluded the GMPE of Zhao et al. (2006) from further analysis, since even after adapting to the available Aegean strong-motion data, it does not properly account for back-arc and fore-arc differences of the observed strong-motion levels (see Skarlatoudis, 2017). This is most probably the reason that this GMPE exhibits the higher RMS level when fitting the available macroseismic data. It is clear that the Skarlatoudis GMPE is compatible with a larger (**M**=8.3) and deeper event (h=130 km) in the broader Santorini-Anafi area, while the adapted BCHydro model is also compatible with a shallower, smaller-magnitude event.

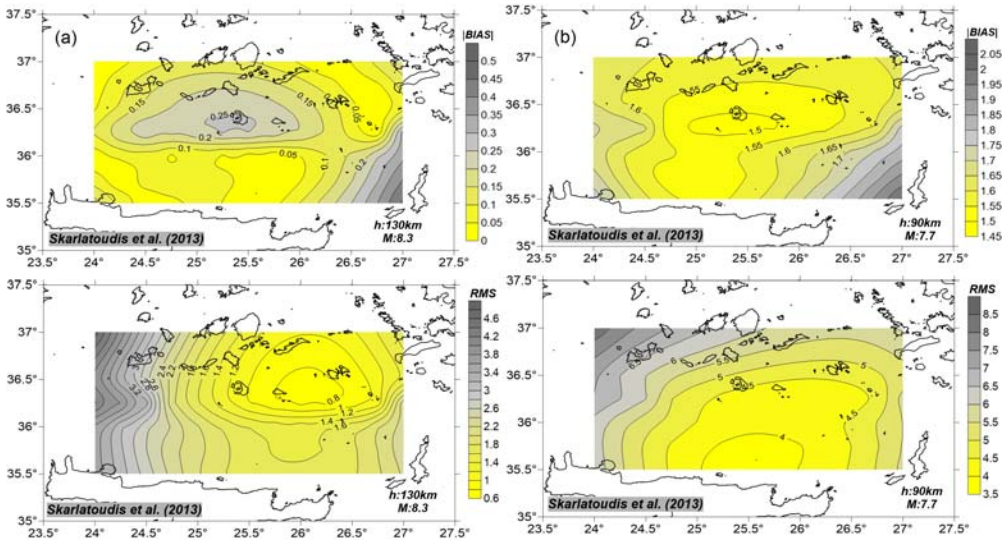

Figure 4. Distribution of RMS and bias values for the macroseismic data of the 1856 event using the GMPE of Skarlatoudis et al. (2013) for two alternative events: a) h=130 km and **M**=8.1 and, b) h=90 km and **M**=7.5.

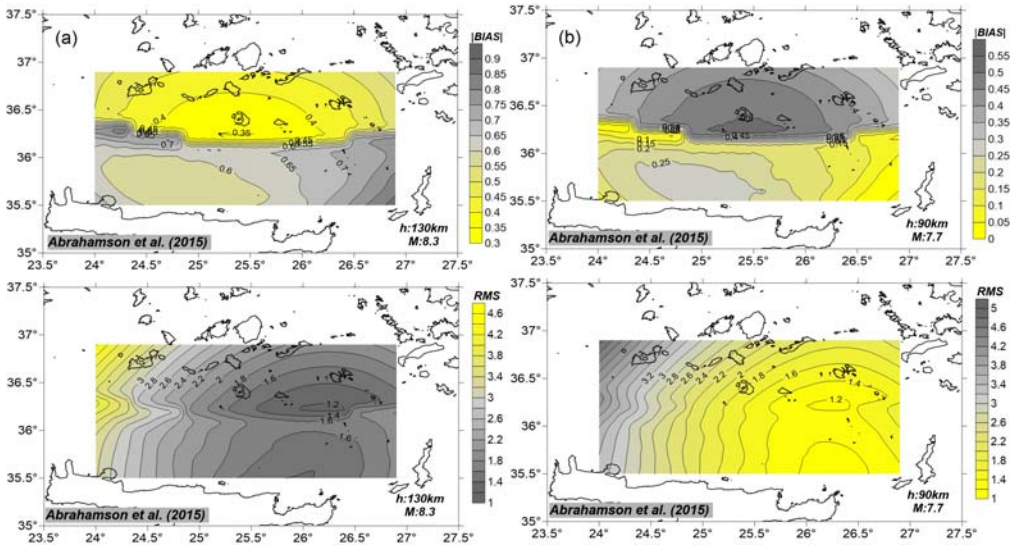

Figure 5. Same as Figure 4 for the BCHydro GMPE, as adapted for the Aegean data by Skarlatoudis (2017).

4. STRONG GROUND-MOTION MODELLING

To further examine the two possible epicenters proposed for the 1856 event, we used the finite fault stochastic model (Motazedian and Atkinson, 2005), as modified by Boore (2009) and implemented in the EXSIM_DMB code. The employed approach is based on the study of Kkallas et al. (2018a), which was also used for the stochastic simulation of several 20th century intermediate-depth earthquakes in

the southern Aegean Sea using their macroseismic information (Kkallas et al., 2018b). In this approach, the anelastic attenuation functions developed from the GMPE of Skarlatoudis et al. (2013) were implemented to constrain the different attenuation patterns and properties for the back-arc and fore-arc area. Furthermore, the same study has used the high-frequency spectral-slope dataset of Ventouzi et al. (2015), to constrain the near-source high frequency spectral slopes, κ_0.

Table 1. Parameters used in the stochastic simulations

Parameter	**Value for M=7.7**		**Value for M=8.3**	
Shear wave velocity (Vs)	4.56 km/s		4.56 km/s	
Density (ρ)	3.22 Kg/m^3		3.22 Kg/m^3	
Geometric spreading: Rb: b=	-1 (All Distances)		-1 (All Distances)	
Anelastic attenuation model	Following Kkallas et al. (2018a)	As shown in Figure 7a (3D Attenuation model)	Following Kkallas et al. (2018a)	As shown in Figure 7b (3D Attenuation model)
Fault plane orientation	Strike: 346^o, Dip:58^o, Ztor=68 km (Figure 3d)		Strike: 340^o, Dip:49^o, Ztor=34 km (Figure 3d)	
Fault length and width	64 km x 64 km		120 km x 120 km	
Rupture propagation speed	0.8Vs		0.8Vs	
Stress parameter	800 bars (Kkallas et al., 2018b)		1600 bars (Estimated from Kkallas et al., 2018b)	
Subfault source duration	$1/f_0$, where f_0 is the subfault corner frequency.		$1/f_0$, where f_0 is the subfault corner frequency.	
Slip distribution	Random		Random	

The fault dimensions for the considered event were estimated using the results from Kkallas et al. (2018a), who proposed the use of equal fault length and width (equation 2) for southern Aegean Sea intermediate-depth earthquakes.

$$ln\ D = 1.03\ M - 3.8 \quad (2)$$

In Figure 3d we present the adopted focal mechanisms for the two (2) examined earthquake scenarios, as well as the selected fault planes depicted with black solid lines, while in Table 1 the dimensions of the selected fault and a summary of several modeling parameters is given. Both considered intermediate-depth earthquakes are associated with strike–slip faulting, with a significant thrust component. From the proposed location and the Benioff-zone geometry, a depth of 130 km was assigned to the first earthquake. We also used the focal mechanism determined by Brüstle et al. (2014) for the 1956 aftershock, which occurred roughly in the same location. For the second location scenario, a representative focal mechanism proposed by Kkallas et al. (2013) for this area was considered, having the typical pattern of P-axis parallel to the local strike of the Hellenic Arc and a T-axis normal to the same strike and parallel to the down-dip direction of the Benioff zone. Both fault planes were selected on the basis of the preferred intermediate-depth fault orientations proposed by Papazachos (1996).

For the simulations, the effect of local site conditions on seismic motions needs to be taken into account. Since we have a re-digitized isoseismal map and not the original IDP information, we made the realistic assumption that the initial isoseismal map (Figure 2) was also based on macroseismic intensities values reported for different site conditions. Therefore, we also incorporated site-effects in our simulations, using V_{S30} estimates (shear wave velocity averaged over the top 30 meters) from topographic slope proxies, following the approach Wald and Allen (2007) that has been shown to be also applicable for the area of Greece (Stewart et al., 2014). From the calculated V_{S30} values, generic amplification functions proposed for A/B, C and D NEHRP soil formations in Greece were employed for the modeling (Margaris and Boore, 1998, Klimis et al., 1999, 2006). All

simulations of the present study were performed for both magnitudes of **M**=8.1-8.3, since smaller magnitudes resulted in high RMS and bias values between the observed and synthetic macroseismic intensities.

As earlier described, the adopted approach of Kkallas et al. (2018a) employed back-arc and fore-arc attenuation functions based on the GMPE modeling of Skarlatoudis et al. (2013). In the present work, we also used an alternative approach, by employing the 3D Q_S model developed by Ventouzi et al. (2015). More specifically for each source-site path we computed the total-path attenuation time from this Q_S model and used-it to define the high-frequency attenuation, κ, value. In this way, two stochastic simulations were performed for each examined hypocenter scenario, each one with different high-frequency spectral decay values.

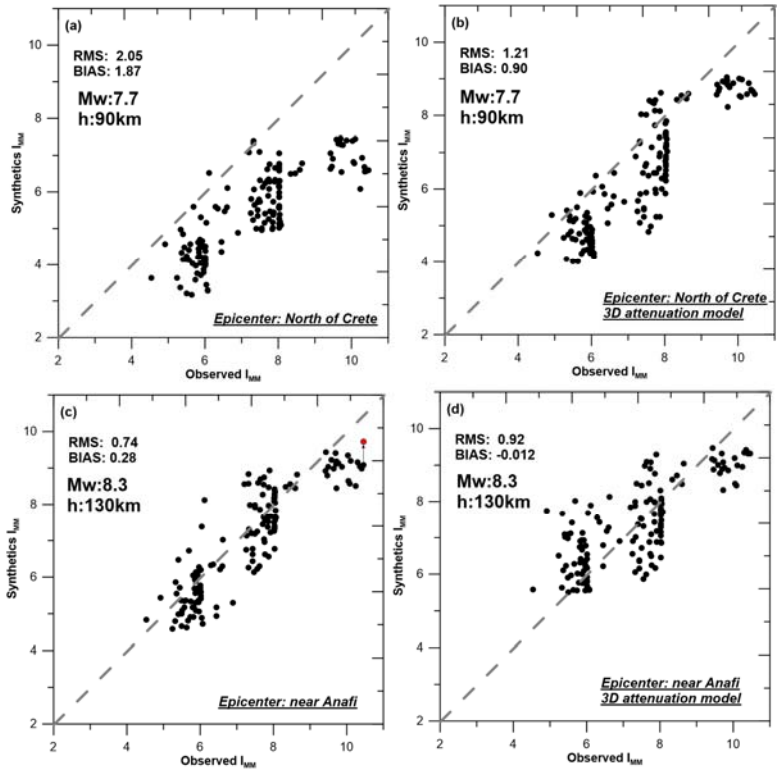

Figure 6. Comparison of the modelled, *I*, versus the digitized (from isoseismals), *Iobs*, macroseismic intensities for the 1856 earthquake. a) Earthquake epicenter north of Crete using the approach of Kkallas et al. (2018a). b) Same epicenter using the total-path kappa values estimates from the 3D Q_S attenuation model of Ventouzi et al (2015). c) and d) Same as (a) and (b), respectively, for the alternative epicenter, close to the island of Anafi. The red circle in (c) corresponds to an updated intensity assessment for the city of Heraklion using locally available transfer functions (see text for explanation).

Figure 6 presents a comparison of the spatial distribution of the 169 digitized IDP data [compatible with the Sieberg (1932) isoseismals] and the corresponding modelled intensities, for the two attenuation models and the two proposed epicenters near Crete and Anafi. Figure 6a shows the spatial distribution following the original Kkallas et al. (2018a) approach when the epicenter is located near Crete, while Figure 6b shows the results for the same epicenter when incorporating high-frequency total-path spectral slopes determined for this event from the 3D Q_S attenuation model, as they are presented in Figure 7a. Figures 6c and 6d present the same results for the alternative earthquake epicenter, near the island of Anafi. It should be considered that as the position of the epicenter changes, the total-path kappa values determined from the 3D Q_S attenuation model also change, as can be seen from Figure 7b. The results presented in Figure 6 suggest that an **M**=8.3 deeper (h=130km) event with an epicenter near Anafi seems to give the optimal results (smaller RMS and bias values).

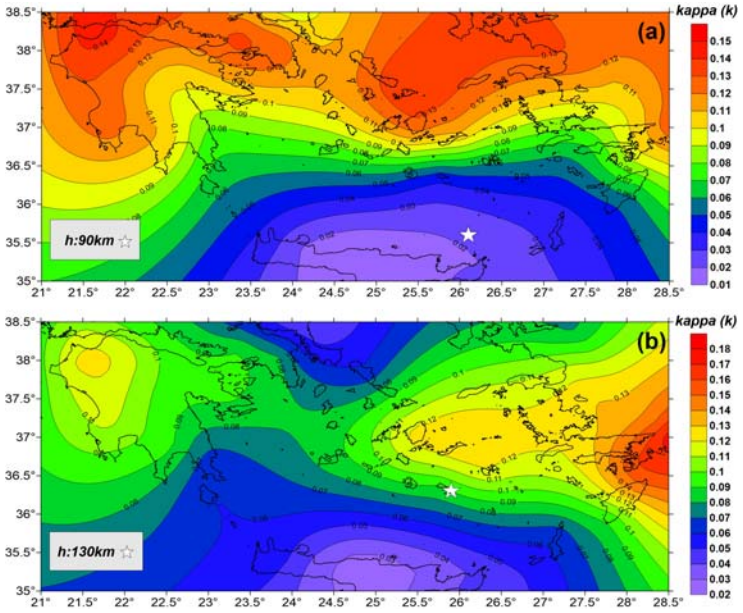

Figure 7. Spatial distribution of total-path κ (kappa) high-frequency attenuation values derived from the 3D Q_S attenuation model proposed by Ventouzi et al. (2015) for two epicenters considered in this work (depicted with white stars): a) Epicenter near the island of Crete (h=90 km) and, b) alternative epicenter, near of the island of Anafi (h=130 km).

5. MODEL EVALUATION

Despite the relatively small number of instrumental data available for strong intermediate-depth events, historical data (e.g. macroseismic information and verbal reports) can be used to investigate these events in more detail. The combined application of Ground-Motion Prediction Equations (GMPEs) and stochastic simulation methods in the present work allowed us not only to better constraint the possible epicenter for the 1856 event, but also provides additional information on how to better simulate the "anomalous" macroseismic intensity pattern observed for this type of earthquakes. More specifically, the results obtained in the present study show that there is an increased possibility for the 1856 event to be located near of the island of Anafi (h~130 km, **M**=8.3), as this is indicated by the smaller RMS and bias values between observed and predicted macroseismic intensity values calculated using the examined approaches. It is interesting to notice that an intermediate-depth earthquake occurred in the same epicentral area roughly 100 years later (1956, h>100 km) with relatively smaller magnitude (**M**~6.9, Brüstle et al., 2014), supporting the proposed scenario.

Moreover, the results of our study suggest while several approaches can be employed to estimate the stong-motion and/or damage distributions from large-magnitude historical intermediate-depth events (various GMPE, stochastic simulations, etc.), their application needs to be carefully evaluated, as some can only be applied under certain conditions. A typical example can be seen in the results obtained in the present work for the modified equations of Abrahamson et al. (2015), as adapted for the Aegean by Skarlatoudis (2017). As seen in Figures 3b and 5b, the use of this GMPE leads to 2 possible clusters of epicenters, with an acceptable RMS and bias between observed and modeled intensities. To explain the source of this double solution, we present in Figure 8 two predictions for the same epicenter near Anafi (h: 130km) for an a) **M**=8.0 and, b) **M**=8.1 event. The results indicate the presence of a problem in the performance of this GMPE for large magnitude events (as the ones examined in this work), since the estimated intensity values for the larger earthquake **M**=8.1 event are significantly smaller than the corresponding values for the smaller earthquake (**M**=8.0). This change of behavior for **M**>8.0 is due to the fact that the magnitude-term of the original BCHydro GMPE was modified by Skarlatoudis (2017) only for **M**<8.0 for the Aegean area, as the corresponding dataset contained data in the range **M**5.1-6.7. As a result, a “break” in the adapted GMPE predictions is observed above and below **M**=8.0, resulting in the pattern observed in Figure (8). This discrepancy suggests that the application of the adapted Abrahamson et al. (2015) BCHydro relation, as proposed by Skarlatoudis

(2017), for large magnitude events (M~7.5-8.5) should not be employed, until further analysis has resolved the introduced bias.

Similar conclusions can be reached for the recently proposed 3D tomographic attenuation model for the area by Ventouzi et al. (2015). The obtained results from the performed simulation suggests that it cannot constrain the high-frequency spectral attenuation for deep earthquake (h=130 km) in the Aegean, exhibiting systematically larger RMS values in the case examined (figure 6d). On the other hand, the model performs adequately for the shallower depth event (h=90 km, figure 6b), leading to more realistic results, as can be confirmed by the comparison of the modelled, I, against observed, Iobs, macroseismic intensities (figure 6a). This behavior is most probably due to the fact that the model predicts lower total-path kappa (κ) values for the deeper epicenter (see Figure 7), while it is well documented that deeper events in the Aegean exhibit more pronounced back-arc/fore-arc differences due to back-arc attenuation effects (e.g. Skarlatoudis et al., 2013).

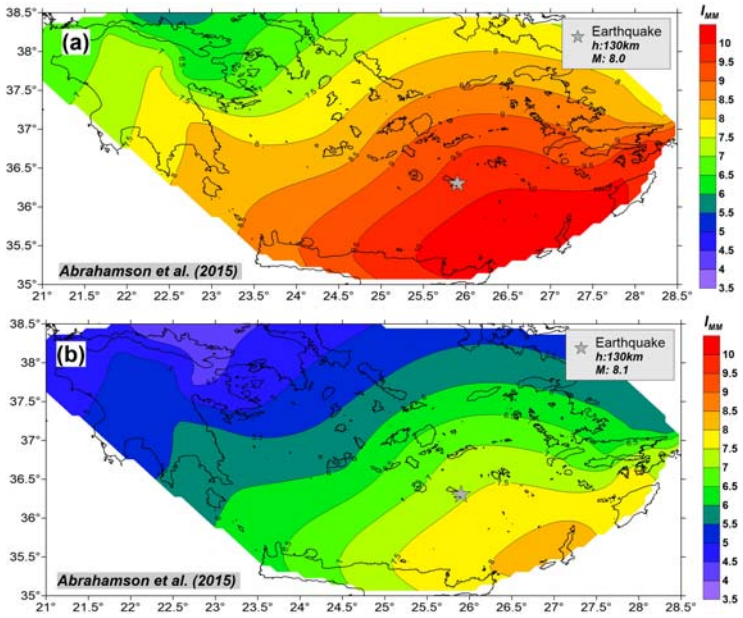

Figure 8. Spatial distribution of the modelled (simulated) macroseismic intensity values for two cases with epicenter near Anafi a) **M**=8.0, h=130 km and b) **M**=8.1, h=130 km. The star denotes the epicenter of the earthquake.

6. CONCLUSIONS

Figure 9 presents the spatial distribution of synthetic macroseismic intensities calculated with the stochastic simulation approach proposed by Kkallas et al (2018a) for the two proposed epicenters (near Crete and near Anafi). The results of Figure 9a confirm the intermediate-depth character of the 1856 event, showing a strongly varying spatial pattern is observed, with maximum macroseismic intensities (up to ~9.5) in the northern east and central coasts of Crete, in very good correlation with the distribution presented in Figure 2. Intensity values less than 6.5 are observed for the largest part of the back-arc area (e.g. Cyclades and neighboring islands). While the distribution pattern of Figure 9b is not very different, it is evident that it cannot capture several features observed in Figure 2 and Figure 9a, such as the observation of peak intensity values in northern Crete, the low intensities in the eastern Aegean back-arc area (e.g. Kos island), the presence of significant intensities in western Crete (Chania area, etc.).

The main problem of the distribution presented in Figure 9a are the maximum predicted intensities for northern Crete, which appear to underestimate the maximum observed intensity values (~10) observed in main urban center like e.g. Heraklion. This is also observed in Figure 6c, where the largest systematic bias between observations and predictions is observed for intensities larger than 9. This bias can be partly due to the generic approach adopted for the site-effect assessment, which fails to

predict the behavior of the deep Neogene deposits of northern Crete in cities like Heraklion (e.g. Savvaidis et al., 2014) and Chania (Pelekis and Athanasopoulos, 2013; Papadopoulos et al., 2017). To confirm this suggestion, we employed in the stochastic simulations the transfer functions proposed for the city of Heraklion from Grendas et al. (2017), instead of the generic ones used in Figure 9a. The new transfer functions have resulted in an increase of ~0.7 intensity units for the simulated site (city of Heraklion). The updated synthetic intensity is depicted with a red circle in Figure 6c, showing a much better agreement between predicted and observed intensities. This observation confirms that the bias observed in Figure 6c for high-intensities in northern Crete may be due to the approximate handling of site-effects in our simulations. Moreover, it suggests that efficient damage assessment for large intermediate-depth magnitude events in the southern Aegean area requires the incorporation of site-effects with the use of realistic, local transfer functions.

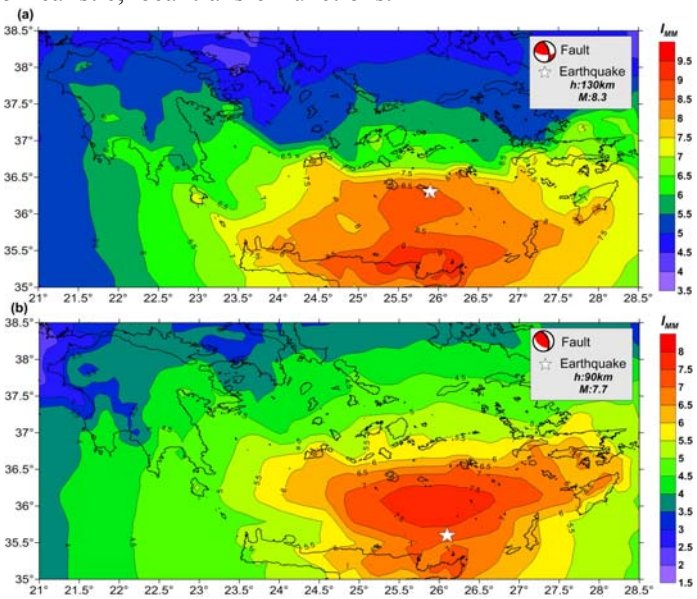

Figure 9. Spatial distribution of the modelled (simulated) macroseismic intensity values for the 1856 earthquake (12 Oct 1856, **M**=8.3) for a) epicenter near Anafi and depth (h=130 km) and b) epicenter near Crete and depth (h=90 km). The fault plane used for the simulation is shown with the thick black solid line and the epicenter is depicted by the solid white star.

7. REFERENCES

Abrahamson, N., Gregor, N., and Addo, K. (2015). BC Hydro Ground Motion Prediction Equations for Subduction Earthquakes. *Earthquake Spectra*, 32(1), 23-44.

Boore, D. M. (2009), Comparing Stochastic Point-Source and Finite-Source Ground-Motion Simulations: SMSIM and EXSIM, *Bull. Seism. Soc. Am*., 99(6), 3202-3216.

Brüstle, A., Friederich, W., Meier, T. and Gross, C. (2014). Focal mechanism and depth of the 1956 Amorgos twin earthquakes from waveform matching of analogue seismograms. *Solid Earth*, 5(2), p.1027.

Grendas I., Theodoulidis N., Hatzidimitiou P., Margaris V. and Drouet S., (2017). Determination of site amplification based on non-linear inversion of accelerometric data in Greece. paper presented at 4th International Conference on Earthquake Engineering and Seismology, Eskisehir, Turkey.

Jusseret, S., Langohr, C. and Sintubin, M., 2013. Tracking earthquake archaeological evidence in Late Minoan IIIB (1300–1200 BC) Crete (Greece): A proof of concept.*Bull. Seism. Soc. Am.*, 103(6), pp.3026-3043.

Kkallas, C., K. Papazachos, E. Scordilis, and V. Margaris (2013), Re-examining the stress field of the broader Southern Aegean subduction area using an updated focal mechanism database, *Bull. Geol. Soc. Greece*, 47(2), 563-573, (http://geolib.geo.auth.gr/index.php/bgsg/article/view/10658/10384).

Kkallas, C., C. B. Papazachos, B. N. Margaris, D. M. Boore, Ch. Ventouzi , and A. Skarlatoudis (2018a) Stochastic strong ground motion simulation of the southern Aegean Sea Benioff zone intermediate-depth earthquakes, *Bull. Seism. Soc. Am.*(in press).

Kkallas, C., C. B. Papazachos, D. M. Boore, Ch. Ventouzi , and B. N. Margaris, (2018b) Historical intermediate-depth earthquakes in the southern Aegean Sea benioff zone: modeling their anomalous macroseismic patterns with stochastic ground-motion simulations. *Bulletin of Earthquake Engineering*, submitted.

Klimis, N. S., B. N. Margaris, and P. K. Koliopoulos (1999), Site-dependent amplification functions and response spectra in greece., *Journal of Earthquake Engineering*, 3(02), 237–270.

Klimis, N., Margaris, B., Anastasiadis, A., Koliopoulos P. and Em. Kirtas (2006), Smoothed Hellenic Rock Site Amplification Factors, *5th Hellenic Congress of Geotechnical and Geoenvironmental Engineering*, Vol. 2, p. 239-246, Xanthi, Greece [in Greek].

Margaris, B. N., and D. M. Boore (1998), Determination of $\Delta\sigma$ and $\kappa 0$ from response spectra of large earthquakes in Greece, *Bulletin of the Seismological Society of America*, 88(1), 170-182.

Motazedian, D., and G. M. Atkinson (2005), Stochastic Finite-Fault Modeling Based on a Dynamic Corner Frequency, Bull. Seism. Soc. Am., 95(3), 995-1010, doi:10.1785/0120030207.

Papadopoulos, G. (2011). A seismic history of Crete, Ocelotos Publ., Athens, 385pp.

Papadopoulos, I., Papazachos, C., Savvaidis, A., Theodoulidis, N., Vallianatos, F. (2017). Seismic microzonation of the broader Chania basin area (Southern Greece) from the joint evaluation of ambient noise and earthquake recordings. *Bull. Earth. Eng.*, 15 (3), 861-888.

Papazachos, B., and Papazachou, K. (2003). The earthquakes of Greece – 2nd edition, Ziti Publ., Thessaloniki, 273pp.

Papazachos, B. (1996). Large seismic faults in the Hellenic arc, Ann. Geofisica, 36(5), 891-903.

Papazachos, B.C., Dimitriadis, S.T., Panagiotopoulos, D.G., Papazachos, C.B. and Papadimitriou, E.E. (2005). Deep structure and active tectonics of the southern Aegean volcanic arc, Developments in Volcanology, 7, 47-64.

Pelekis, P.C. and Athanasopoulos, G.A. (2013). Seismic microzonation of Chania, Crete (Greece) based on SASW measurements and non-linear site response analyses. *Soil Dynamics and Earthquake Engineering*, 53, pp.145-159.

Savvaidis, A., Margaris, B., Theodoulidis, N., Lekidis, V., Karakostas, C., Loupasakis, C., Rozos, D., Soupios, P., Mangriotis, M., Dikmen, U. and Tsangaratos, P. (2014). Geo-Characterization at selected accelerometric stations in Crete (Greece) and comparison of earthquake data recordings with EC8 elastic spectra. *Open Geosciences, 6(1),* pp.88-103.

Sieberg, A. (1932), Die Erdbeben. In: Gutenberg, B., Handbuch der Geophysik 4, 93–94, Berlin.

Skarlatoudis, A. A. (2017), Applicability of ground-motion prediction equations to a Greek within-slab earthquake dataset, *Bulletin of Earthquake Engineering*, 1-22.

Skarlatoudis, A.A., C. B. Papazachos, B.N. Margaris, C. Ventouzi, and I. Kalogeras (2013), Ground-Motion Prediction Equations of Intermediate-Depth Earthquakes in the Hellenic Arc, Southern Aegean Subduction Area, *Bull. Seism. Soc. Am.*, 103(3), 1952-1968.

Stewart, J. P., N. Klimis, A. Savvaidis, N. Theodoulidis, E. Zargli, G. Athanasopoulos, P. Pelekis, G. Mylonakis, and B. Margaris (2014), Compilation of a Local VS Profile Database and Its Application for Inference of VS30 from Geologic- and Terrain-Based Proxies, *Bull. Seism. Soc. Am.*, 104(6), 2827-2841, doi:10.1785/0120130331.

Vamvakaris, D. A., Papazachos, C. B., Papaioannou Ch, A., Scordilis, E. M., & Karakaisis, G. F. (2016). Seismic hazard assessment in the broader aegean area using time-independent seismicity models based on synthetic earthquake catalogs. Bulletin of the Geological Society of Greece, 50.

Ventouzi, C., C. B. Papazachos, C. Papaioannou, P. Hatzidimitriou, and the EGELADOS working group (2015), Qp and Qs attenuation models of the southern Aegean subduction area, paper presented at 15th European conference on Earthquake Engineering & 34th General Assembly of the European Seismological Commission, Istanbul, Turkey.

Wald, D. J., and T. I. Allen (2007), Topographic Slope as a Proxy for Seismic Site Conditions and Amplification, *Bulletin of the Seismological Society of America*, 97(5), 1379-1395, doi:10.1785/0120060267.

Zhao, J.X., Zhang, J., Asano, A., Ohno, Y., Oouchi, T., Takahashi, T., Ogawa, H., Irikura, K., Thio, H.K., Somerville, P.G. and Fukushima, Y., 2006. Attenuation relations of strong ground motion in Japan using site classification based on predominant period, *Bull. Seism. Soc. Am.*, 96(3), 898-913.